

# Hierarchical Bayesian Mixture Models for Time Series Using Context Trees as State Space Partitions

Ioannis Papageorgiou<sup>\*</sup>      Ioannis Kontoyiannis<sup>†</sup>

February 4, 2022

## Abstract

A general hierarchical Bayesian framework is introduced for mixture modelling and inference with real-valued time series. At the top level, the state space is partitioned via the choice of a discrete context tree, so that the resulting partition depends on the values of some of the most recent samples. At the bottom level, a different model is associated with each region of the partition. This defines a very rich and flexible class of mixture models, for which we provide algorithms that allow for efficient, *exact* Bayesian inference. In particular, it is shown that the maximum *a posteriori* probability (MAP) model (including the relevant MAP context tree partition) can be precisely identified, along with its exact posterior probability. The utility of this general framework is illustrated in detail when a different autoregressive (AR) model is used in each state-space region, resulting in a mixture-of-AR model class. The performance of the associated algorithmic tools is demonstrated in the problems of model selection and forecasting on both simulated and real-world data, where they are found to provide results as good or better than state-of-the-art methods.

**Keywords.** Time series, Bayesian mixture models, Exact Bayesian inference, State space partitions, Model selection, Forecasting, Autoregressive models, Context trees.

---

<sup>\*</sup>Department of Engineering, University of Cambridge, Trumpington Street, Cambridge CB2 1PZ, UK. Email: [ip307@cam.ac.uk](mailto:ip307@cam.ac.uk).

<sup>†</sup>Statistical Laboratory, Centre for Mathematical Sciences, University of Cambridge, Wilberforce Road, Cambridge CB3 0WB, UK. Email: [yiannis@maths.cam.ac.uk](mailto:yiannis@maths.cam.ac.uk).

# 1 Introduction

Time series modelling, inference and prediction are critical tasks in statistics and machine learning, with a wide range of important applications in areas including economics, finance, neuroscience, communications, ecology, and weather forecasting. Due to the great number of potential applications, a wide variety of modelling approaches have been proposed, with complementary advantages that often depend heavily on the particular application. These include autoregressive (AR) and ARIMA models along with their generalisations, hidden Markov models, state-space models like the stochastic volatility model, deep neural network models, and Gaussian process models. However, there remains a pressing need for more flexible, parsimonious, and rich model classes, that are conceptually simple and suitable for applications with limited training data. This is the motivation for this work, in which we propose a very general class of hierarchical Bayesian mixture models that can utilise any of the above models as a building block.

A flexible and easily interpretable hierarchical Bayesian model for real-valued time series is defined, which at the top level considers partitions of the state space, and at the bottom level associates an arbitrary time series model (like the ones mentioned above) to each region of the partition. The state-space partitions considered at the top level are adaptive (both in “time” and “space”), and are defined in terms of a discretised version of the most recent samples, which we refer to as the *discrete context*. In order to extract the discrete context from real-valued observations, simple quantisers from  $\mathbb{R}$  to a finite alphabet are introduced.

The precise formulation of the state-space partitions is in terms of discrete *context-tree* models, which are shown to be able to represent meaningful and useful partitions, and to enable capturing important aspects of the structure present in the data in a natural manner. Context-tree models (under the name context-tree sources) were introduced by Rissanen (Rissanen, 1983a,b, 1986) as descriptions of variable-memory Markov chains, a generalised class of higher-order Markov chains that admit parsimonious representations. Since then, they have been used widely with discrete-valued time series, mostly in connection with compression (Weinberger et al., 1994; Willems et al., 1995; Willems, 1998), and more recently they have also been studied from a Bayesian statistics point of view (Kontoyiannis et al., 2020; Papageorgiou et al., 2021). However, the role of context trees in the present development for real-valued time series is conceptually very different from its use with discrete time series: traditionally, they are used to capture high-order dependencies in a parsimonious way, while here, by defining partitions of the state space, they are employed as a device for allowing (possibly quite complex) mixtures of different models that already include higher-order dependencies.

The first step in developing tools for performing Bayesian inference for the resulting hierarchical model is an extension of the *Bayesian Context Trees* (BCT) framework of Kontoyiannis et al. (2020), which was found to be very effective in important statistical tasks for discrete time series. This extension mainly consists of three parts: 1) introducing the quantiser to extract discrete contexts from real-valued observations, along with an associated Bayesian inference method for selecting it, 2) placing a prior for a real-valued time series model in each region of the state-space, and, 3) modifying the associated algorithms of Kontoyiannis et al. (2020) for this setting.

This leads to a powerful Bayesian framework for our hierarchical modelling structure, which allows for *exact* and efficient Bayesian inference within this vast model class. In particular, the prior predictive likelihood  $p(x)$  of a time series  $x$ , with all models and parameters integrated out (also known as the *evidence*), can be computed exactly. Furthermore, the *a posteriori* most

likely (MAP) partition can be identified, and its posterior probability can be computed exactly. So, the “best” partition is selected automatically from the data, without employing any *ad hoc* considerations. Also, the Bayesian approach as usual offers a quantitative measure of uncertainty for all relevant results.

To illustrate the application of the general framework, we study in detail the case where autoregressive (AR) models are used as building blocks for the bottom layer, with a different AR model associated to each state-space region. This results in a flexible, nonlinear mixture-of-AR model class, for which it is possible to perform exact Bayesian inference. We refer to this collection of models as the Bayesian context tree autoregressive (BCT-AR) model class. This mixture model is expected to be very effective in standard applications of nonlinear time series analysis in economics and finance.

Regarding comparisons with other benchmarks, our focus will be on approaches that have been used widely and have been found to be most successful for this type of applications. As explained in detail in the experiments’ section, these mainly include popular mixtures of AR models: the threshold autoregressive (TAR) models (Tong, 2011), and the mixture autoregressive (MAR) models (Wong & Li, 2000). In contrast, “data-hungry” nonlinear methods like (deep) neural networks, that naturally involve a large number of parameters, are generally less effective for the kind of problems and datasets considered in this work, as they are severely limited by the relatively small training data sizes. Hence, comparing with such methods is not particularly relevant here. Similarly, extensions of MAR models including the conditional heteroscedastic (MAR-ARCH) model (Wong & Li, 2001b), the use of exogenous variables (Wong & Li, 2001a), and the use of the Student-*t* distribution to model heavy tails (Wong et al., 2009), also seem less relevant, as their benefits are limited to examples of datasets possessing these specific characteristics (conditional heteroskedasticity, heavy tails, etc.).

Finally, we note that a number of alternative approaches have been introduced for employing discrete patterns in the analysis of real-valued time series; see, e.g., Alvarez et al. (2010); Alvisi et al. (2007); Berndt & Clifford (1994); Fu et al. (2007); Hu et al. (2014); Liu et al. (2011); Ouyang et al. (2010); Sabeti et al. (2020). These works illustrate the fact that useful and meaningful information can indeed be extracted from discrete contexts. However, in most cases the methods considered are either application-specific or task-specific, and typically resort to *ad hoc* considerations for performing inference. In sharp contrast, in this work discrete contexts are used in a natural and principled manner, by defining a clean Bayesian modelling structure upon which “orthodox” Bayesian inference is performed.

The rest of this paper is organised as follows. In Section 2, the general hierarchical model that uses context trees as partitions is defined for an arbitrary class of models used at the bottom level. The prior structure and the methodology used for Bayesian inference in this general setting are then described. In Section 3, the AR model is adopted for the bottom level, and all the details of the proposed methodology are given for this case. Also, the resulting BCT-AR mixture model is compared with other commonly used mixture-of-AR models. Finally, in Section 4, its performance in model selection and forecasting is illustrated on simulated data and real-world applications from economics and finance.

## 2 Bayesian context trees for real-valued time series

### 2.1 Discrete contexts

A key element of our development is the definition of a model class for real-valued time series based on extracting discrete contexts from continuous-valued observations. These contexts play the role of discrete-valued feature vectors that can be used to identify additional useful structure in the data. In order to extract these contexts, in this paper we introduce simple piecewise constant quantisers from  $\mathbb{R}$  to a finite alphabet  $A = \{0, 1, \dots, m - 1\}$ , of the form,

$$Q(x) = \begin{cases} 0, & x < c_1, \\ i, & c_i \leq x \leq c_{i+1}, \quad 1 \leq i \leq m - 2, \\ m - 1, & x > c_{m-1}, \end{cases} \quad (1)$$

where, throughout this section, the thresholds  $\{c_1, \dots, c_{m-1}\}$  and the resulting quantiser  $Q$  are considered fixed. A systematic way to infer the thresholds from data is described in Section 3.2.

We note that the general framework described in this section can be used in conjunction with an arbitrary way of extracting discrete features, by considering any mapping to a discrete alphabet, not necessarily of the form in (1). However, the quantisation of course needs to be meaningful in order to lead to useful results. Quantisers as in (1) offer a generally reasonable choice, although, depending on the application at hand, there are other useful approaches, e.g., quantising percentage differences between successive samples.

### 2.2 Context trees as partitions of the state space

Given a quantiser  $Q$  with  $m$  levels as above, a maximum context length  $D \geq 0$ , and a proper  $m$ -ary context tree  $T$ , we define a partition of the state space  $\mathbb{R}^D$  in terms of  $T$  as follows; see (Kontoyiannis et al., 2020) for a detailed description of discrete context tree models  $T$ . For a time series  $x = \{x_n\}$ , let  $t = (Q(x_{n-1}), \dots, Q(x_{n-D}))$  be the discrete context of length  $D$  corresponding to the sample  $x_n$  at time  $n$ , and let  $s$  be the unique leaf of  $T$  that is a suffix of  $t$ . For example, for the context tree of Figure 1, if  $Q(x_{n-1}) = 0$  and  $Q(x_{n-2}) = 1$  then  $s = 01$ , whereas if  $Q(x_{n-1}) = Q(x_{n-2}) = 1$  then  $s = 1$ . This defines a partition of  $\mathbb{R}^2$  into three regions indexed by the contexts  $\{1, 01, 00\}$  corresponding to the leaves of the tree  $T$ .

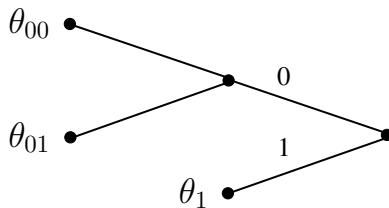


Figure 1: Example of a binary context tree  $T$  used for representing the state space partition

To complete the specification of the hierarchical model, we associate a different model to each leaf  $s$  of the context tree  $T$ , giving a different conditional density for  $x_n$ : At time  $n$ , given the context  $s$  determined by the past  $D$  samples  $(x_{n-1}, \dots, x_{n-D})$ , the distribution of  $x_n$  is given by the model assigned to  $s$ . Although general non-parametric models could also be used, for the rest of this paper we consider parametric models with parameters  $\theta_s$  at each leaf  $s$ .

So, for the example of Figure 1, denoting  $x^{n-1}$  the past samples  $\{x_{n-1}, x_{n-2}, \dots\}$ , and  $c$  the threshold of the binary quantiser  $Q$ ,

$$p(x_n|T, \theta, x^{n-1}) = \begin{cases} p_{\theta_1}(x_n|x^{n-1}), & \text{if } s = 1, \\ p_{\theta_{01}}(x_n|x^{n-1}), & \text{if } s = 01, \\ p_{\theta_{00}}(x_n|x^{n-1}), & \text{if } s = 00, \end{cases}$$

with  $s = 1$  if  $x_{n-1} > c$ ,  $s = 01$  if  $x_{n-1} \leq c$ ,  $x_{n-2} > c$ , and  $s = 00$  if  $x_{n-1} \leq c$ ,  $x_{n-2} \leq c$ .

As in Kontoyiannis et al. (2020), we consider partitions represented by context trees  $T$  in the collection  $\mathcal{T}(D)$  of all proper  $m$ -ary trees with depth no greater than  $D$ . A tree  $T$  is proper if any node in  $T$  that is not a leaf has exactly  $m$  children. Here, this means that proper trees define proper partitions, so that the resulting state space regions are disjoint and their union is the whole space  $\mathbb{R}^D$ .

Altogether, given a tree  $T \in \mathcal{T}(D)$ , to each leaf  $s$  we associate a parameter vector  $\theta_s$  that specifies the corresponding parametric model at  $s$ .

For a time series  $x$  consisting of observations  $(x_1, x_2, \dots, x_n)$  together with an initial segment  $(x_{-D+1}, \dots, x_0)$  of length  $D$ , we write  $x_i^j$  for the segment  $x_i, x_{i+1}, \dots, x_j$ , for  $i \leq j$ . Viewing  $T$  as the collection of its leaves, the likelihood induced by this hierarchical model is,

$$p(x_1^n|T, \theta, x_{-D+1}^0) = \prod_{i=1}^n p(x_i|T, \theta, x_{-D+1}^{i-1}) = \prod_{s \in T} \prod_{i \in B_s} p(x_i|T, \theta_s, x_{-D+1}^{i-1}), \quad (2)$$

where  $B_s$  is the set of indices  $i \in \{1, 2, \dots, n\}$  such that the context of  $x_i$  is  $s$ , and  $\theta = \{\theta_s ; s \in T\}$ .

### 2.3 Bayesian modelling and inference

**Prior structure.** For the trees  $T \in \mathcal{T}(D)$  with maximum depth  $D \geq 0$  at the top level of the hierarchical model, we use the BCT prior of Kontoyiannis et al. (2020),

$$\pi(T) = \pi_D(T; \beta) = \alpha^{|T|-1} \beta^{|T|-L_D(T)}, \quad (3)$$

where  $\beta \in (0, 1)$  is a hyperparameter,  $\alpha$  is given by  $\alpha = (1 - \beta)^{1/(m-1)}$ ,  $|T|$  is the number of leaves of  $T$ , and  $L_D(T)$  is the number of leaves  $T$  has at depth  $D$ . This prior clearly penalises larger trees corresponding to more complex models by an exponential amount. Given a tree model  $T \in \mathcal{T}(D)$ , we place an independent prior on each  $\theta_s$ , so that  $\pi(\theta|T) = \prod_{s \in T} \pi(\theta_s)$ .

For a time series  $x = \{x_n\}$ , one of the main quantities of interest in terms of inference is the partition posterior distribution,  $\pi(T|x) = p(x|T)\pi(T)/p(x)$ . It is well known that the main obstacle in performing Bayesian inference is the computation of the normalising constant  $p(x)$ :

$$p(x) = \sum_{T \in \mathcal{T}(D)} \pi(T) p(x|T). \quad (4)$$

The power of the proposed Bayesian structure comes, in part, from that fact that, although  $\mathcal{T}(D)$  is enormously rich, consisting of doubly-exponentially many models in  $D$ , it is possible to compute  $p(x)$  precisely, thus making it possible to perform *exact* Bayesian inference efficiently. As we show below, the BCT methodology of Kontoyiannis et al. (2020) can in fact be extended to this setting, and generalisations of the corresponding algorithms can be used to compute the normalising factor of (4) and to identify the *a posteriori* most likely trees.

The main requirement for being able to use this methodology is that the parameters  $\theta$  be easy to integrate out, so that the marginal likelihoods  $p(x|T)$  can be factorised as,

$$p(x|T) = \int p(x|\theta, T)\pi(\theta|T) d\theta = \prod_{s \in T} P_e(s, x), \quad (5)$$

for some explicit function  $P_e(s, x)$  of the data  $x = \{x_n\}$  and the context  $s$ . Note that, under our assumptions, the marginal likelihoods  $p(x|T)$  can always be expressed as:

$$p(x|T) = \int p(x|\theta, T)\pi(\theta|T) d\theta = \int \prod_{s \in T} \prod_{i \in B_s} p(x_i|T, \theta_s, x_{-D+1}^{i-1}) \prod_{s \in T} \pi(\theta_s) \prod_{s \in T} d\theta_s.$$

So, what we actually need is to be able to compute the *estimated probabilities*  $P_e(s, x)$ , defined by:

$$P_e(s, x) = \int \prod_{i \in B_s} p(x_i|T, \theta_s, x_{-D+1}^{i-1}) \pi(\theta_s) d\theta_s. \quad (6)$$

When this is possible, modified versions of the algorithms of [Kontoyiannis et al. \(2020\)](#) can be used for efficient, exact inference, where now the estimated probabilities  $P_e(s, x)$  of (6) are to be used in place of their discrete versions. In this line, here we introduce the Continuous Context Tree Weighting (CCTW) algorithm, and the Continuous Bayesian Context Tree (CBCT) algorithm. It is shown that CCTW can be used to compute the normalising constant  $p(x)$  (Theorem 1), and CBCT can be used to identify the MAP partition (Theorem 2). The proofs of these theorems are similar to those in the discrete case, and are given in Appendix A. The  $k$ -BCT algorithm of [Kontoyiannis et al. \(2020\)](#) can also be modified in an analogous manner to give the top- $k$  *a posteriori* most likely partitions, but it is not shown here as its description is quite lengthy.

Let  $x = x_{-D+1}^n$  be a time series, and let  $y_i = Q(x_i)$  denote the corresponding quantised samples.

#### **CCTW: Continuous context tree weighting algorithm**

1. Build the tree  $T_{\text{MAX}}$ , whose leaves are all the discrete contexts  $y_{i-D}^{i-1}$ ,  $i = 1, 2, \dots, n$ . Compute  $P_e(s, x)$  as given in (6) for each node  $s$  of  $T_{\text{MAX}}$ .
2. Starting at the leaves and proceeding recursively towards the root compute:

$$P_{w,s} = \begin{cases} P_e(s, x), & \text{if } s \text{ is a leaf,} \\ \beta P_e(s, x) + (1 - \beta) \prod_{j=0}^{m-1} P_{w,sj}, & \text{o/w,} \end{cases}$$

where  $s_j$  is the concatenation of context  $s$  and symbol  $j$ .

#### **CBCT: Continuous Bayesian context tree algorithm**

1. Build the tree  $T_{\text{MAX}}$  and compute  $P_e(s, x)$  for each node  $s$  of  $T_{\text{MAX}}$ , as in CCTW.
2. Starting at the leaves and proceeding recursively towards the root compute:

$$P_{m,s} = \begin{cases} P_e(s, x), & \text{if } s \text{ is a leaf at depth } D, \\ \beta, & \text{if } s \text{ is a leaf at depth } < D, \\ \max \{ \beta P_e(s, x), (1 - \beta) \prod_{j=0}^{m-1} P_{m,sj} \}, & \text{o/w.} \end{cases}$$

3. Starting at the root and proceeding recursively with its descendants, for each node  $s$ : if the maximum above is achieved by the first term, prune all its descendants from  $T_{\text{MAX}}$ .

**Theorem 1.** *The weighted probability  $P_{w,s}$  at the root is exactly the normalising constant  $p(x)$  of (4).*

**Theorem 2.** *For all  $\beta \geq 1/2$ , the tree  $T_1^*$  produced by the CBCT algorithm is the MAP tree model.*

Even in cases where the integrals in (6) are not tractable, they may be easy to compute approximately. Then, the above algorithms could be used with these approximations as a way of performing approximate inference. However, in this paper we do not investigate this further. Instead, we illustrate the general principle via an interesting example where these integrals can be computed explicitly and the resulting mixture model is a flexible model of practical interest. This is described in the next section, where the AR model is used as the parametric model associated to each region. We refer to the resulting hierarchical model as the Bayesian context tree autoregressive (BCT-AR) model.

### 3 The Bayesian context tree autoregressive model

Here we consider the hierarchical model where each leaf  $s$  corresponds to an AR model of order  $p$ ,

$$x_n = \phi_{s,1}x_{n-1} + \cdots + \phi_{s,p}x_{n-p} + e_n = \boldsymbol{\phi}_s^T \tilde{\mathbf{x}}_{n-1} + e_n,$$

with  $e_n \sim \mathcal{N}(0, \sigma_s^2)$ ,  $\boldsymbol{\phi}_s = (\phi_{s,1}, \dots, \phi_{s,p})^T$ , and  $\tilde{\mathbf{x}}_{n-1} = (x_{n-1}, \dots, x_{n-p})^T$ .

In this case the parameters of the model are the AR coefficients and the noise variance, so that  $\theta_s = (\boldsymbol{\phi}_s, \sigma_s^2)$ . We use an inverse-gamma prior for the noise variance, and a Gaussian prior for the AR coefficients, so that the joint prior on the parameters is  $\pi(\theta_s) = \pi(\boldsymbol{\phi}_s | \sigma_s^2) \pi(\sigma_s^2)$ , with,

$$\pi(\sigma_s^2) = \text{Inv-Gamma}(\tau, \lambda), \quad (7)$$

$$\pi(\boldsymbol{\phi}_s | \sigma_s^2) = \mathcal{N}(\boldsymbol{\mu}_o, \sigma_s^2 \boldsymbol{\Sigma}_o), \quad (8)$$

where  $(\tau, \lambda, \boldsymbol{\mu}_o, \boldsymbol{\Sigma}_o)$  are the prior hyperparameters.

This prior specification allows the exact computation of the estimated probabilities  $P_e(s, x)$  of (6), and also gives closed-form posteriors for the AR coefficients and the noise variance. These are given in Lemmas 1 and 2, which are proven in Appendix B.

**Lemma 1.** *For the AR model, the estimated probabilities  $P_e(s, x)$  as in (6) are given by,*

$$P_e(s, x) = C_s^{-1} \frac{\Gamma(\tau + |B_s|/2) \lambda^\tau}{\Gamma(\tau) (\lambda + D_s/2)^{\tau + |B_s|/2}}, \quad (9)$$

where  $|B_s|$  is the cardinality of the set  $B_s$  in (2), i.e., the number of observations with context  $s$ , and,

$$C_s = \sqrt{(2\pi)^{|B_s|} \det(I + \boldsymbol{\Sigma}_o S_3)},$$

$$D_s = \mathbf{s}_1 + \boldsymbol{\mu}_o^T \boldsymbol{\Sigma}_o^{-1} \boldsymbol{\mu}_o - (\mathbf{s}_2 + \boldsymbol{\Sigma}_o^{-1} \boldsymbol{\mu}_o)^T (S_3 + \boldsymbol{\Sigma}_o^{-1})^{-1} (\mathbf{s}_2 + \boldsymbol{\Sigma}_o^{-1} \boldsymbol{\mu}_o),$$

with the sums  $s_1$ ,  $\mathbf{s}_2$  and  $S_3$  defined as:

$$s_1 = \sum_{i \in B_s} x_i^2, \quad \mathbf{s}_2 = \sum_{i \in B_s} x_i \tilde{\mathbf{x}}_{i-1}, \quad S_3 = \sum_{i \in B_s} \tilde{\mathbf{x}}_{i-1} \tilde{\mathbf{x}}_{i-1}^T.$$

**Lemma 2.** *Given a tree model  $T$ , at each leaf  $s$ , the posterior distributions of the AR coefficients and the noise variance are given by,*

$$\pi(\sigma_s^2|T, x) = \text{Inv-Gamma}(\tau + |B_s|/2, \lambda + D_s/2), \quad (10)$$

$$\pi(\phi_s|T, x) = t_\nu(\mathbf{m}_s, P_s), \quad (11)$$

where  $t_\nu$  denotes a multivariate  $t$ -distribution with  $\nu$  degrees of freedom. Here,  $\nu = 2\tau + |B_s|$ , and,

$$\mathbf{m}_s = (S_3 + \Sigma_o^{-1})^{-1}(\mathbf{s}_2 + \Sigma_o^{-1}\mu_o), \quad (12)$$

$$P_s^{-1} = \frac{2\tau + |B_s|}{2\lambda + D_s}(S_3 + \Sigma_o^{-1}). \quad (13)$$

**Corollary.** *The MAP estimators of  $\phi_s$  and  $\sigma_s^2$  are given, respectively, by,*

$$\widehat{\phi}_s^{\text{MAP}} = \mathbf{m}_s, \quad \widehat{\sigma}_s^2{}^{\text{MAP}} = (2\lambda + D_s)/(2\tau + |B_s| + 2). \quad (14)$$

### 3.1 Computational complexity and sequential updates

For a time series  $x_1^n$ , with an initial segment  $x_{-D+1}^0$ , the tree  $T_{\text{MAX}}$  has no more than  $nD + 1$  nodes. For each symbol  $x_i$  in  $x_1^n$ , exactly  $D + 1$  nodes of  $T_{\text{MAX}}$  need to be updated, corresponding to its contexts of length  $0, 1, \dots, D$ . For each one of these nodes, only the quantities  $\{|B_s|, s_1, s_2, S_3\}$  need to be updated, which can be done efficiently by just adding an extra term to each sum. Using these and Lemma 1, the estimated probabilities  $P_e(s, x)$  can be computed for all nodes of  $T_{\text{MAX}}$  (i.e., with a constant number of operations for each node). Also, the recursive step only performs operations on  $T_{\text{MAX}}$ . So, as a function of  $n$  and  $D$ , the complexity of all three algorithms is only  $\mathcal{O}(nD)$ : **linear** in the length of the time series and the maximum depth considered. This is particularly important, giving empirical running times of no more than a second in all our experiments (using a simple implementation in a common laptop). Also, it means that our methods scale very well with large numbers of observations.

Another important observation is that it is possible to perform sequential updates efficiently. For example, consider observing a new sample  $x_{n+1}$  after executing CCTW for  $x_1^n$ . As above, only  $D + 1$  nodes need to be updated, corresponding to the contexts of  $x_{n+1}$ . In particular,  $P_e(s, x)$  and  $P_{w,s}$  need to be updated *only* at these nodes, taking  $\mathcal{O}(D)$  operations in total, i.e.,  $\mathcal{O}(1)$  as a function of  $n$ .

### 3.2 Choosing the hyperparameters, quantiser and autoregressive order

It can be seen from Lemma 2 that the posterior distributions of  $\phi_s$  and  $\sigma_s^2$  are typically not very sensitive to the prior hyperparameters (i.e., when reasonably many observations exist with context  $s$ ). In all the experimental results below we make the simple choice  $\mu_o = 0$  and  $\Sigma_o = I$  in the AR coefficients' prior. For  $\tau$  and  $\lambda$ , in view of equation (10), they should be chosen to be relatively small in order to minimise their effect on the posterior, while keeping the mode of the inverse-gamma prior,  $\lambda/(\tau + 1)$ , reasonable. For the context tree prior, we use the default value of  $\beta = 1 - 2^{-m+1}$  (Kontoyiannis et al., 2020), and the maximum depth  $D = 10$ .

Finally, we need to specify the way in which the quantiser thresholds  $\{c_i\}$  of (1) and the AR order  $p$  are chosen. We do this in a Bayesian manner by considering the thresholds and the order as parameters on an additional layer, above everything else. Placing uniform priors

on  $\{c_i\}$  and  $p$ , we can perform standard Bayesian model selection, as in, e.g., [Rasmussen & Ghahramani \(2001\)](#); [MacKay \(1992\)](#); [Rasmussen & Williams \(2006\)](#). The resulting posterior  $p(\{c_i\}, p|x)$  is proportional to the *evidence*  $p(x|\{c_i\}, p)$ , which can be calculated *exactly* using the CCTW algorithm ([Theorem 1](#)).

So, in order to select appropriate values, we can simply choose a collection of possible  $\{c_i\}$  and  $p$ , and select the ones with the higher evidence. For the AR order we take  $1 \leq p \leq p_{\max}$  for an appropriate  $p_{\max}$ , and for the  $\{c_i\}$  we perform a grid search in a reasonable range (e.g., between the 10th and 90th percentiles of the data).

Even though we use a uniform prior for  $p, \{c_i\}$ , the Bayesian approach implicitly penalises more complex models by averaging over more parameters. This is well-known (e.g., [Rasmussen & Ghahramani \(2001\)](#); [MacKay \(1992\)](#); [Smith & Spiegelhalter \(1980\)](#); [Kass & Raftery \(1995\)](#)) and is often referred to as “automatic Occam’s Razor”. In fact, the popular BIC model selection criterion ([Schwarz, 1978](#)) can be derived as an asymptotic approximation to the evidence ([Konishi & Kitagawa, 2008](#)).

### 3.3 Comparison with other autoregressive mixtures

Having completed the specification of the BCT-AR model, we compare its properties with other popular AR mixtures.

**Threshold autoregressive models.** Threshold autoregressive (TAR) models were introduced in [Tong & Lim \(1980\)](#), and have been used extensively in the analysis of nonlinear time series; see, e.g., the review papers ([Tong, 2011](#); [Hansen, 2011](#)) and the texts ([Cryer & Chan, 2008](#); [Tsay, 2005](#); [Tong, 1990](#)). Although numerous different versions of TAR models have been employed (see, e.g., the discussion in [Tong \(2011\)](#)), the most commonly used one is the self-exciting threshold autoregressive (SETAR) model, given by,

$$x_n = \phi_1^{(j)} x_{n-1} + \dots + \phi_p^{(j)} x_{n-p} + \sigma^{(j)} e_n, \quad \text{if } Q(x_{n-d}) = j \in A, \quad (15)$$

where  $e_n \sim \mathcal{N}(0, 1)$ ,  $p$  is the autoregressive order,  $Q: \mathbb{R} \rightarrow A = \{0, \dots, m-1\}$  is an  $m$ -ary quantiser of the form in [\(1\)](#), and  $d$  is called the *delay* parameter. So, the SETAR model considers partitions of the state space based on the value of  $x_{n-d}$ , with different parameters  $(\phi^{(j)}, \sigma^{(j)})$  associated to each region.

**Mixture autoregressive models.** The mixture autoregressive (MAR) models of [Wong & Li \(2000\)](#) are a generalisation of the Gaussian mixture transition distribution (GMTD) models of [Le et al. \(1996\)](#), consisting of a simple mixture of  $K$  Gaussian AR components. Specifically, the conditional cumulative distribution function (CDF) of  $X_n$  given its past  $x^{n-1} = \{x_{n-1}, x_{n-2}, \dots\}$ , is given by,

$$F(x_n|x^{n-1}) = \sum_{k=1}^K \alpha_k \Phi\left(\frac{x_n - \phi_1^{(k)} x_{n-1} \dots - \phi_{p_k}^{(k)} x_{n-p_k}}{\sigma_k}\right)$$

where  $K$  is the number of components,  $\Phi$  is the CDF of the standard normal distribution, each component has order  $p_k$ , and the weights satisfy  $\alpha_k > 0$ ,  $\alpha_1 + \dots + \alpha_K = 1$ .

The BCT-AR model introduced above can be viewed as a strict **generalisation** of both the MAR and SETAR model classes. First, note that the simple AR model is always included in  $\mathcal{T}(D)$  as the empty tree consisting only of the root node. The general SETAR partitions in [\(15\)](#) are also always contained in  $\mathcal{T}(D)$  since they only depend on a quantised version of  $x_{n-d}$  with a quantiser  $Q$  of the form [\(1\)](#). So, it is obvious that the BCT-AR model class is more general.

Also, when the BCT-AR posterior concentrates on  $K$  trees,  $T_1, \dots, T_K$ , (which was commonly observed in practice), the posterior predictive distribution can be written as,

$$p(x_{n+1}|x) = \sum_{k=1}^K \pi(T_k|x) p(x_{n+1}|T_k, x),$$

so that BCT-AR can be viewed as a generalised MAR model, with components corresponding to the AR models at the leaves of each  $T_k$ , and with Bayesian weights determined by the posterior as  $\pi(T_k|x)$ .

In view of the above discussion, the model class induced by the context trees  $\mathcal{T}(D)$  is a rich, flexible collection of nonlinear models that are appropriate for at least as many applications as those where SETAR or MAR models are employed. Some important advantages of this approach are that (1) it allows for effective, exact Bayesian inference; and (2) it implicitly overcomes important challenges that arise naturally with SETAR and MAR models. Specifically, selecting the delay and threshold parameters, the AR order, and the number of components (for SETAR and MAR models respectively), are challenging tasks that require involved procedures that often need to be carried out in an *ad hoc* manner (see, e.g., [Cryer & Chan \(2008\)](#); [Wong & Li \(2000\)](#); [Tong \(2011\)](#)). In the BCT-AR framework, these can be viewed as parameters of the Bayesian model, facilitating principled procedures for their choices, as described earlier.

## 4 Experiments

### 4.1 Simulated data

We first present the results of an experiment based on simulated data, illustrating that our methods are consistent and effective on data generated by a model in our class. The context tree model used here is the tree of [Figure 1](#), the threshold for the (binary) quantiser is  $c = 0$ , and the AR order is  $p = 2$ .

The exact model is given by:

$$x_n = \begin{cases} 0.7x_{n-1} - 0.3x_{n-2} + e_n, & e_n \sim \mathcal{N}(0, 0.15), \text{ if } s = 1, \\ -0.3x_{n-1} - 0.2x_{n-2} + e_n, & e_n \sim \mathcal{N}(0, 0.1), \text{ if } s = 01, \\ 0.5x_{n-1} + e_n, & e_n \sim \mathcal{N}(0, 0.05), \text{ if } s = 00, \end{cases}$$

with  $s = 1$  if  $x_{n-1} > 0$ ,  $s = 01$  if  $x_{n-1} \leq 0$ ,  $x_{n-2} > 0$ , and  $s = 00$  if  $x_{n-1} \leq 0$ ,  $x_{n-2} \leq 0$ .

The generated dataset and the code used can be found in the supplementary material. The hyperparameter values are  $\beta = 0.5$ ,  $D = 10$ ,  $\mu_o = 0$ ,  $\Sigma_o = I$ ,  $\lambda = 1.0$ ,  $\tau = 1.0$ .

We first examine the posterior over trees,  $\pi(T|x)$ . On a time series consisting of only  $n = 100$  observations, the MAP tree identified by the CBCT algorithm is the empty tree corresponding to a single AR model, with posterior probability 99.9%. This means that the data do not provide sufficient evidence to support a more complex partition. With  $n = 300$  observations, the MAP tree is now the true underlying model, with posterior probability 57%. And with  $n = 500$  observations, the posterior of the true model is 99.9%. Therefore, the posterior indeed concentrates on the true model, indicating that the BCT-AR inferential framework can be very effective even on small datasets.

The model fitted from  $n = 1000$  observations, using the MAP parameters from [\(14\)](#), is:

$$x_n = \begin{cases} 0.66x_{n-1} - 0.19x_{n-2} + e_n, & e_n \sim \mathcal{N}(0, 0.16), \\ -0.39x_{n-1} - 0.27x_{n-2} + e_n, & e_n \sim \mathcal{N}(0, 0.12), \\ 0.45x_{n-1} - 0.03x_{n-2} + e_n, & e_n \sim \mathcal{N}(0, 0.058), \end{cases}$$

in the corresponding regions  $s = 1$ ,  $s = 01$ , and  $s = 00$ .

This shows that all estimated parameters are very close to their true value, as desired. More details on parameter estimation can be found in Appendix C, where it is shown that with  $n = 10^4$  observations all estimators have essentially converged. Error bars are also reported there as posterior standard deviations, which are reduced with more samples, verifying convergence.

In the results above, the correct values of the quantiser threshold  $c = 0$  and the AR order  $p = 2$  were used. Next, we apply the procedure described in Section 3.2 for choosing  $c$  and  $p$  based on the data. The results of Table 1 show that the evidence  $p(x|c,p)$  is maximised at the true values of  $c$  and  $p$ , verifying that our inferential procedure is effective.

Table 1: Using the evidence  $p(x|c,p)$  to choose the AR order and the quantiser threshold

	AR order $p$					Threshold $c$				
	1	2	3	4	5	-0.1	-0.05	0	0.05	0.1
$-\log_2 p(x c,p)$	533	<b>519</b>	526	531	535	558	539	<b>519</b>	555	577

## 4.2 The stock price of IBM

As a first real-world example, we study the daily IBM common stock closing price from May 17, 1961 to November 2, 1962 (369 observations), taken from Box et al. (2015). This is a well-studied dataset, analysed, e.g., in Box et al. (2015); Tong (1990); Makridakis et al. (1998); Le et al. (1996); Wong & Li (2000); it is contained in the R package ‘fma’ (Hyndman, 2020). Initially, an ARIMA (0,1,1) model was fitted to the time series (Box et al., 2015), given by  $x_n = x_{n-1} + e_n - 0.09 e_{n-1}$ , where  $e_n \sim \mathcal{N}(0, 52.2)$ . This model was found to be ineffective, partly because of its inability to incorporate nonlinearities, indicating SETAR (Tong, 1990) as a better candidate. The best-BIC SETAR model was found to have 2 regions separated by a threshold of 0 for the return series:  $x_{n-1} > x_{n-2}$  and  $x_{n-1} \leq x_{n-2}$ . Then, a GMTD model was found to give a better fit to this data in Le et al. (1996), and a MAR model with three components was subsequently used in Wong & Li (2000), which was determined to be superior.

We fit a BCT-AR model to the first-difference time series  $\Delta x_n = x_n - x_{n-1}$ . For the discrete context we choose a ternary quantiser with values  $\{0, 1, 2\}$ , corresponding to “states” {down, steady, up}. The specifics of the procedure followed (as outlined in Section 3.2) to select the thresholds, AR order, and hyperparameters can be found in Appendix D, and relevant code can be found in the supplementary material. The resulting quantiser regions are:  $s = 0$  if  $\Delta x_{n-1} < -7$ ,  $s = 2$  if  $\Delta x_{n-1} > 7$ , and  $s = 1$  otherwise.

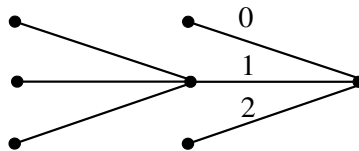


Figure 2: MAP tree model

The MAP tree identified by CBCT is shown in Figure 2. Its posterior is 99.3%, which is perhaps somewhat remarkable: it means there is very strong evidence supporting this exact structure, even with only 369 observations. The resulting model for the original time series  $x_n$ ,

with its MAP parameters, is given below, where  $e_n \sim \mathcal{N}(0, 1)$ ,

$$x_n = \begin{cases} 1.03 x_{n-1} - 0.03 x_{n-2} + 12.3 e_n, & \text{if } s = 0, \\ 1.17 x_{n-1} - 0.17 x_{n-2} + 6.86 e_n, & \text{if } s = 2, \\ -0.11 x_{n-1} + 1.11 x_{n-2} + 10.8 e_n, & \text{if } s = 10, \\ 1.22 x_{n-1} - 0.22 x_{n-2} + 5.32 e_n, & \text{if } s = 11, \\ 0.15 x_{n-1} + 0.85 x_{n-2} + 5.17 e_n, & \text{if } s = 12. \end{cases}$$

This model reveals important information about apparent structure in the data, which has not been identified before. Firstly, it admits a very simple and natural interpretation: in order to determine the AR model generating the next value, we need to look back until there is a significant enough price change (corresponding to contexts 0, 2, 10, 12), or until we reach the maximum depth of 2 (context 11).

Another important feature captured by this model is the commonly observed asymmetric response in volatility due to positive and negative shocks, sometimes called “the leverage effect” (Tsay, 2005; Box et al., 2015). Even though there is no suggestion of that in the prior, the MAP model shows that negative shocks increase the volatility much more: context 0 has the highest volatility, with 10 being a close second, showing that the effect of a past shock is still present. Finally, we observe that when stabilising after a shock (contexts 10, 12), the latest value  $x_{n-1}$  is not as important as  $x_{n-2}$ , whereas  $x_{n-1}$  is dominant in all other cases.

As the most successful among earlier approaches is the MAR model of Wong & Li (2000), we follow the procedure of Wong & Li (2000) and compare the BCT-AR model with the MAR, SETAR and ARIMA models in terms of its ability to describe the predictive distribution of the series. Specifically, one-step prediction intervals (PIs) are constructed, and their empirical coverages (i.e., the percentage of data falling within them) are computed. From the results of Table 2 we see that BCT-AR performs much better than ARIMA and SETAR, as the empirical coverages of the resulting PIs are much closer to the nominal values. Compared to MAR, the BCT-AR performance is at least comparable, if not better.

Table 2: Empirical coverages of prediction intervals

Model	Coverages of % prediction intervals				
	90%	80%	70%	60%	50%
ARIMA	<b>90.22</b>	83.97	77.72	69.84	57.34
SETAR	90.47	83.38	76.84	69.75	58.86
MAR	89.37	80.93	<b>70.30</b>	61.58	51.50
BCT-AR	89.34	<b>80.87</b>	72.40	<b>59.84</b>	<b>50.82</b>

### 4.3 US unemployment rate

An important application of TAR models is in modelling the US unemployment rate (Hansen, 2011). In Montgomery et al. (1998); Tsay (2005), the quarterly US unemployment rate from 1948 to 1993 was studied in detail. As described there, it moves countercyclically with US business cycles, and rises quickly but decays slowly, indicating nonlinear behavior. In order to capture these features, a SETAR model was fitted to the dataset, which had order  $p = 2$ , and two regions. The first region corresponds to a decrease or minor increase in the unemployment

rate, signifying a stable economy, and the second region corresponds to jumps of 0.1 or higher, indicating economic contractions. This model, together with a seasonal ARIMA (1,1,0) (4,0,4) model, had the best performance in forecasting.

We consider the quarterly US unemployment rate in the longer period from 1948 to 2019 (288 observations), which is publicly available from the Bureau of Labor Statistics ([https://data.bls.gov/timeseries/LNS14000000?years\\_option=all\\_years](https://data.bls.gov/timeseries/LNS14000000?years_option=all_years)). For the SETAR model, we use the R package TSA (Chan & Ripley, 2020), along with the popular conditional least squares method (Chan, 1993). For the seasonal ARIMA and MAR models we use the R packages ‘forecast’ (Hyndman & Khandakar, 2008) and ‘mixAR’ (Boshnakov & Ravagli, 2021).

Following Montgomery et al. (1998) and Tsay (2005), we consider the difference series  $\Delta x_n = x_n - x_{n-1}$ , and also include a constant term in the AR model. Additional details can be found in Appendix E, and relevant code in the supplementary material. As discussed above, a binary quantiser is a natural choice here, so that 0 corresponds to a decrease or minor increase (stable economy), and 1 corresponds to jumps (economic contractions). The threshold selected using the procedure of Section 3.2 is  $c = 0.15$ . Comparing with SETAR, this slightly higher threshold seems more suitable for detecting contractions. The resulting MAP tree is the tree of Figure 1, with leaves  $\{1, 01, 00\}$ , and posterior 91.5%. The complete BCT-AR model with its MAP parameters is,

$$\Delta x_n = \begin{cases} 0.09 + 0.72\Delta x_{n-1} - 0.30\Delta x_{n-2} + 0.42 e_n, \\ 0.04 + 0.29 \Delta x_{n-1} - 0.32 \Delta x_{n-2} + 0.32 e_n, \\ -0.02 + 0.34 \Delta x_{n-1} + 0.19 \Delta x_{n-2} + 0.20 e_n, \end{cases}$$

with  $e_n \sim \mathcal{N}(0, 1)$ , and corresponding regions  $s = 1$  if  $\Delta x_{n-1} > 0.15$ ,  $s = 01$  if  $\Delta x_{n-1} \leq 0.15$ ,  $\Delta x_{n-2} > 0.15$ , and  $s = 00$  if  $\Delta x_{n-1} \leq 0.15$ ,  $\Delta x_{n-2} \leq 0.15$ .

The BCT-AR MAP model appears to find significant additional structure in the data compared with SETAR. It consists of 3 regions, hence identifying an additional relevant “state”. Jumps higher than 0.15 correspond to economic contractions (context 1), but if the most recent state is not a jump the model looks further back to determine the next state. Context 00 corresponds to a stable economy, but context 01 now identifies a new state: “stabilising just after a contraction”. The volatility in each case is as expected: higher in contractions, smaller in stable economy regions, and in-between for context 01.

Table 3: Mean squared error (MSE) of forecasts

Model	Prediction step				
	1	2	3	4	5
Seas. ARIMA	5.40	7.71	10.1	11.6	11.0
SETAR	5.42	8.34	8.82	9.48	9.95
MAR	5.33	7.61	8.92	9.56	9.71
BCT-AR	<b>4.90</b>	<b>7.33</b>	<b>8.44</b>	<b>9.08</b>	<b>9.48</b>

Following Montgomery et al. (1998); Tsay (2005), we evaluate the performance of all models in forecasting, considering 1-step to 5-step ahead forecasts. The training set consists of the first 50% of the observations, and we also allow sequential updates. For BCT-AR, at every timestep we use the MAP tree with its MAP parameters, which can be updated efficiently

(Section 3.1). For multi-step-ahead forecasts, we use the parametric bootstrap of Tsay (2005): we sample trajectories from the model, and use the sample average as the point forecast. The results of Table 3 clearly show that the BCT-AR predictor performs much better than the other methods. It achieves the lowest mean squared error (MSE) in all five cases, with a significant difference between 3.8% and 8.8% from the second-best method. In conclusion, the BCT-AR model performs significantly better in prediction than state-of-the-art methods, and it also provides important additional information for the structure present in the data.

## 5 Concluding remarks

This work develops a very rich and general Bayesian mixture model class for real-valued time series, that considers partitions of the state space at the top level and fits a different model to each region at the lower level. It is accompanied by a collection of methodological and algorithmic tools for exact Bayesian inference within this class of models. The general framework, when AR models are used at the bottom layer, is shown to lead to a flexible, nonlinear mixture model (the BCT-AR model), which generalises popular AR mixtures and facilitates efficient, *exact* Bayesian inference. The performance of the proposed methods was illustrated on simulated and real data, and it was found to outperform some of the most commonly used approaches.

The main requirement potentially limiting the applicability of the methods described in this paper is that the “estimated probabilities” of (6) need to be evaluated. This leads to several possible directions for future work. First, as discussed in Section 2.3, when this is not possible explicitly, the integrals in (6) could be computed numerically, leading to approximate inference. So, more general models, e.g., ARMA, ARIMA, ARCH, or even non-parametric models like Gaussian processes could be used at the bottom layer. Also, more general classes of quantisers can be considered for extracting discrete contexts (see Section 2.1), allowing greater flexibility in the state space partitions and enabling the identification of more complex dependencies in the data. Lastly, extending our methods to multivariate time series is also feasible, and would greatly broaden the scope of applications of the hierarchical Bayesian model.

## References

- Alvarez, F., Troncoso, A., Riquelme, J., and Ruiz, J. Energy time series forecasting based on pattern sequence similarity. *IEEE Transactions on Knowledge and Data Engineering*, 23(8): 1230–1243, 2010.
- Alvisi, S., Franchini, M., and Marinelli, A. A short-term, pattern-based model for water-demand forecasting. *Journal of Hydroinformatics*, 9(1):39–50, 2007.
- Berndt, D. and Clifford, J. Using dynamic time warping to find patterns in time series. In *KDD Workshop*, volume 10, pp. 359–370. Seattle, WA, USA, 1994.
- Boshnakov, G. N. and Ravagli, D. *mixAR: Mixture Autoregressive Models*, 2021. R package version 0.22.5. <https://CRAN.R-project.org/package=mixAR>.
- Box, G., Jenkins, G., Reinsel, G., and Ljung, G. *Time series analysis: forecasting and control*. John Wiley & Sons, 2015.
- Chan, K. Consistency and limiting distribution of the least squares estimator of a threshold autoregressive model. *Annals of Statistics*, 21(1):520–533, 1993.
- Chan, K. and Ripley, B. *TSA: Time Series Analysis*, 2020. R package version 1.3. <https://CRAN.R-project.org/package=TSA>.
- Cryer, J. and Chan, K. *Time series analysis: with applications in R*. Springer Science & Business Media, 2008.
- Fu, T., Chung, F., Luk, R., and Ng, C. Stock time series pattern matching: Template-based vs. rule-based approaches. *Engineering Applications of Artificial Intelligence*, 20(3):347–364, 2007.
- Hansen, B. Threshold autoregression in economics. *Statistics and its Interface*, 4(2):123–127, 2011.
- Hu, Q., Su, P., Yu, D., and Liu, J. Pattern-based wind speed prediction based on generalized principal component analysis. *IEEE Transactions on Sustainable Energy*, 5(3):866–874, 2014.
- Hyndman, R. and Khandakar, Y. Automatic time series forecasting: the forecast package for R. *Journal of Statistical Software*, 26(3):1–22, 2008. <https://CRAN.R-project.org/package=forecast>.
- Hyndman, R. J. *fma: Data sets from "Forecasting: methods and applications" by Makridakis, Wheelwright & Hyndman (1998)*, 2020. R package version 2.4. <https://cran.r-project.org/package=fma>.
- Kass, R. and Raftery, A. Bayes factors. *Journal of the American Statistical Association*, 90(430):773–795, 1995.
- Konishi, S. and Kitagawa, G. *Information criteria and statistical modeling*. Springer Science & Business Media, 2008.

- Kontoyiannis, I., Mertzanis, L., Panotopoulou, A., Papageorgiou, I., and Skoularidou, M. Bayesian Context Trees: Modelling and exact inference for discrete time series. *arXiv preprint arXiv:2007.14900*, 2020.
- Le, N., Martin, R., and Raftery, A. Modeling flat stretches, bursts outliers in time series using mixture transition distribution models. *Journal of the American Statistical Association*, 91(436):1504–1515, 1996.
- Liu, X., Ni, Z., Yuan, D., Jiang, Y., Wu, Z., Chen, J., and Yang, Y. A novel statistical time-series pattern based interval forecasting strategy for activity durations in workflow systems. *Journal of Systems and Software*, 84(3):354–376, 2011.
- MacKay, D. Bayesian interpolation. *Neural Computation*, 4(3):415–447, 1992.
- Makridakis, S., Wheelwright, S., and Hyndman, R. *Forecasting: methods and applications*. John Wiley & Sons, 1998.
- Montgomery, A., Zarnowitz, V., Tsay, R., and Tiao, G. Forecasting the US unemployment rate. *Journal of the American Statistical Association*, 93(442):478–493, 1998.
- Ouyang, G., Dang, C., Richards, D., and Li, X. Ordinal pattern based similarity analysis for eeg recordings. *Clinical Neurophysiology*, 121(5):694–703, 2010.
- Papageorgiou, I., Kontoyiannis, I., Mertzanis, L., Panotopoulou, A., and Skoularidou, M. Revisiting context-tree weighting for Bayesian inference. In *2021 IEEE International Symposium on Information Theory (ISIT)*, pp. 2906–2911, 2021. doi: 10.1109/ISIT45174.2021.9518189.
- Rasmussen, C. and Ghahramani, Z. Occam’s razor. *Advances in Neural Information Processing Systems*, pp. 294–300, 2001.
- Rasmussen, C. and Williams, C. *Gaussian processes for machine learning*. MIT Press, 2006.
- Rissanen, J. A universal data compression system. *IEEE Transactions on Information Theory*, 29(5):656–664, 1983a.
- Rissanen, J. A universal prior for integers and estimation by minimum description length. *Annals of Statistics*, 11(2):416–431, 1983b.
- Rissanen, J. Complexity of strings in the class of markov sources. *IEEE Transactions on Information Theory*, 32(4):526–532, 1986.
- Sabeti, E., Song, P., and Hero, A. Pattern-based analysis of time series: Estimation. In *2020 IEEE International Symposium on Information Theory (ISIT)*, pp. 1236–1241, 2020.
- Schwarz, G. Estimating the dimension of a model. *Annals of Statistics*, 6(2):461–464, 1978.
- Smith, A. and Spiegelhalter, D. Bayes factors and choice criteria for linear models. *Journal of the Royal Statistical Society: Series B (Methodological)*, 42(2):213–220, 1980.
- Tong, H. *Non-linear time series: a dynamical system approach*. Oxford University Press, 1990.
- Tong, H. Threshold models in time series analysis—30 years on. *Statistics and its Interface*, 4(2):107–118, 2011.

- Tong, H. and Lim, K. Threshold autoregression, limit cycles and cyclical data. *Journal of the Royal Statistical Society: Series B (Statistical Methodology)*, 42(3):245–268, 1980.
- Tsay, R. *Analysis of financial time series*, volume 543. John Wiley & Sons, 2005.
- Weinberger, M., Merhav, N., and Feder, M. Optimal sequential probability assignment for individual sequences. *IEEE Transactions on Information Theory*, 40(2):384–396, 1994.
- Willems, F. The context-tree weighting method: extensions. *IEEE Transactions on Information Theory*, 44(2):792–798, 1998.
- Willems, F., Shtarkov, Y., and Tjalkens, T. The context-tree weighting method: basic properties. *IEEE Transactions on Information Theory*, 41(3):653–664, 1995.
- Wong, C. S. and Li, W. K. On a mixture autoregressive model. *Journal of the Royal Statistical Society: Series B (Statistical Methodology)*, 62(1):95–115, 2000.
- Wong, C. S. and Li, W. K. On a logistic mixture autoregressive model. *Biometrika*, 88(3): 833–846, 2001a.
- Wong, C. S. and Li, W. K. On a mixture autoregressive conditional heteroscedastic model. *Journal of the American Statistical Association*, 96(455):982–995, 2001b.
- Wong, C. S., Chan, W. S., and Kam, P. L. A student t-mixture autoregressive model with applications to heavy-tailed financial data. *Biometrika*, 96(3):751–760, 2009.

# Appendix

## A Proofs of Theorems 1 and 2

The proofs of Theorems 1 and 2 follow along the same lines as the proofs of the corresponding results for discrete time series in [Kontoyiannis et al. \(2020\)](#). The main change comes from the different form of the estimated probabilities  $P_e(s, x)$  used to factorise the marginal likelihoods  $p(x|T)$  as,

$$p(x|T) = \int p(x|\theta, T)\pi(\theta|T) d\theta = \prod_{s \in T} P_e(s, x). \quad (16)$$

Before giving the proofs of the theorems, we recall a useful property for the BCT prior  $\pi_D(T)$ . Let  $\Lambda = \{\lambda\}$  denote the empty tree consisting only of the root node  $\lambda$ . Any tree  $T \neq \Lambda$  can be expressed as the union  $T = \cup_j T_j$  of a collection of  $m$  subtrees  $T_0, T_1, \dots, T_{m-1}$ , and its prior can be decomposed as ([Kontoyiannis et al., 2020](#)):

**Lemma A.** *If  $T \in \mathcal{T}(D)$ ,  $T \neq \Lambda$ , is expressed as the union  $T = \cup_j T_j$  of the subtrees  $T_j \in \mathcal{T}(D-1)$ , then,*

$$\pi_D(T) = \alpha^{m-1} \prod_{j=0}^{m-1} \pi_{D-1}(T_j). \quad (17)$$

### A.1 Proof of Theorem 1

The proof is by induction. We want to show that:

$$P_{w,\lambda} = p(x) = \sum_{T \in \mathcal{T}(D)} \pi(T)p(x|T) = \sum_{T \in \mathcal{T}(D)} \pi_D(T) \prod_{s \in T} P_e(s, x). \quad (18)$$

We claim that the following more general statement holds: For any node  $s$  at depth  $d$  with  $0 \leq d \leq D$ , we have,

$$P_{w,s} = \sum_{U \in \mathcal{T}(D-d)} \pi_{D-d}(U) \prod_{u \in U} P_e(su, x), \quad (19)$$

where  $su$  denotes the concatenation of contexts  $s$  and  $u$ .

Clearly (19) implies (18) upon taking  $s = \lambda$  (i.e., with  $d = 0$ ). Also, (19) is trivially true for nodes  $s$  at level  $D$ , since it reduces to the fact that  $P_{w,s} = P_{e,s}$  for leaves  $s$ , by definition.

Suppose (19) holds for all nodes  $s$  at depth  $d$  for some fixed  $0 < d \leq D$ . Let  $s$  be a node at depth  $d-1$ ; then, by the inductive hypothesis,

$$\begin{aligned} P_{w,s} &= \beta P_e(s, x) + (1 - \beta) \prod_{j=0}^{m-1} P_{w,sj} \\ &= \beta P_e(s, x) + (1 - \beta) \prod_{j=0}^{m-1} \left[ \sum_{T_j \in \mathcal{T}(D-d)} \pi_{D-d}(T_j) \prod_{t \in T_j} P_e(sjt, x) \right], \end{aligned}$$

where  $sjt$  denotes the concatenation of context  $s$ , then symbol  $j$ , then context  $t$ , in that order.

So,

$$\begin{aligned} P_{w,s} &= \beta P_e(s, x) + (1 - \beta) \sum_{T_0, T_1, \dots, T_{m-1} \in \mathcal{T}(D-d)} \prod_{j=0}^{m-1} \left[ \pi_{D-d}(T_j) \prod_{t \in T_j} P_e(sjt, x) \right] \\ &= \beta P_e(s, x) + \frac{1 - \beta}{\alpha^{m-1}} \sum_{T_0, T_1, \dots, T_{m-1} \in \mathcal{T}(D-d)} \pi_{D-d+1}(\cup_j T_j) \left[ \prod_{j=0}^{m-1} \prod_{t \in T_j} P_e(sjt, x) \right], \end{aligned}$$

where for the last step we have used (17) from Lemma A.

Concatenating every symbol  $j$  with every leaf of the corresponding tree  $T_j$ , we end up with all the leaves of the larger tree  $\cup_j T_j$ . Therefore,

$$P_{w,s} = \beta P_e(s, x) + \frac{1 - \beta}{\alpha^{m-1}} \sum_{T_0, T_1, \dots, T_{m-1} \in \mathcal{T}(D-d)} \pi_{D-d+1}(\cup_j T_j) \prod_{t \in \cup_j T_j} P_e(st, x),$$

and since  $1 - \beta = \alpha^{m-1}$  and  $\pi_d(\Lambda) = \beta$  for all  $d \geq 1$ ,

$$\begin{aligned} P_{w,s} &= \pi_{D-d+1}(\Lambda) P_e(s, x) + \sum_{T_0, T_1, \dots, T_{m-1} \in \mathcal{T}(D-d)} \pi_{D-d+1}(\cup_j T_j) \prod_{t \in \cup_j T_j} P_e(st, x) \\ &= \pi_{D-d+1}(\Lambda) P_e(s, x) + \sum_{T \in \mathcal{T}(D-d+1), T \neq \Lambda} \pi_{D-d+1}(T) \prod_{t \in T} P_e(st, x) \\ &= \sum_{T \in \mathcal{T}(D-d+1)} \pi_{D-d+1}(T) \prod_{t \in T} P_e(st, x). \end{aligned}$$

This establishes (19) for all nodes  $s$  at depth  $d - 1$ , completing the inductive step and the proof of the theorem.  $\square$

## A.2 Proof of Theorem 2

As the proof follows very much along the same lines as that of Theorem 3.2 of Kontoyiannis et al. (2020), most of the details are omitted here.

The proof is again by induction. First, we claim that:

$$P_{m,\lambda} = \max_{T \in \mathcal{T}(D)} p(x, T) = \max_{T \in \mathcal{T}(D)} \pi_D(T) \prod_{s \in T} P_e(s, x). \quad (20)$$

As in the proof of Theorem 1, in fact we claim that the following more general statement holds: For any node  $s$  at depth  $d$  with  $0 \leq d \leq D$ , we have,

$$P_{m,s} = \max_{U \in \mathcal{T}(D-d)} \pi_{D-d}(U) \prod_{u \in U} P_e(su, x), \quad (21)$$

where  $su$  denotes the concatenation of contexts  $s$  and  $u$ . The proof of this is by an inductive step similar to that of Theorem 1. Taking  $s = \lambda$  in (21) implies (20).

Then, it is sufficient to show that for the tree  $T_1^*$  that is produced by the CBCT algorithm,  $P_{m,\lambda} = p(x, T_1^*)$ . This is again proved by induction, via an argument similar to the ones in the previous two cases.

Finally, using (20) and dividing both sides with  $p(x)$  completes the proof, since we get:

$$\max_{T \in \mathcal{T}(D)} \pi(T|x) = \pi(T_1^*|x).$$

$\square$

### A.3 The $k$ -BCT algorithm

The  $k$ -BCT algorithm of [Kontoyiannis et al. \(2020\)](#) can be generalised in a similar manner to the way the CTW and BCT algorithms were generalised. The resulting algorithm identifies the top- $k$  *a posteriori* most likely context-tree partitions. The proof of the theorem claiming this is similar to the proof of Theorem 3.3 of [Kontoyiannis et al. \(2020\)](#) and thus omitted. Again, the important difference, both in the algorithm description and in the proof, is that the estimated probabilities  $P_e(s, x)$  are used in place of their discrete version  $P_e(a_s)$ .

## B Proofs of Lemmas 1 and 2

The proofs of these Lemmas are mostly based on explicit computations. Recall that, for each context  $s$ , the set  $B_s$  consists of those indices  $i \in \{1, 2, \dots, n\}$  such that the context of  $x_i$  is  $s$ . The important step in the following two proofs is the factorisation of the likelihood using the sets  $B_s$ . In order to prove the lemmas for the AR model with parameters  $\theta_s = (\phi_s, \sigma_s^2)$ , we first consider an intermediate step in which we assume the noise variance to be known and equal to  $\sigma^2$ .

### B.1 Known noise variance

Here, to any leaf  $s$  of the context tree  $T$ , we associate an AR model with known variance  $\sigma^2$ , so that,

$$x_n = \phi_{s,1}x_{n-1} + \dots + \phi_{s,p}x_{n-p} + e_n = \phi_s^\top \tilde{\mathbf{x}}_{n-1} + e_n, \quad e_n \sim \mathcal{N}(0, \sigma^2). \quad (22)$$

In this setting, the parameters of the model are only the AR coefficients  $\theta_s = \phi_s$ . For these, we use a Gaussian prior,

$$\theta_s \sim \mathcal{N}(\mu_o, \Sigma_o), \quad (23)$$

where  $\mu_o, \Sigma_o$  are hyperparameters. In this setting we prove the following for the estimated probabilities  $P_e(s, x)$ .

**Lemma B.** *The estimated probabilities  $P_e(s, x)$  for the known-variance case are given by,*

$$P_e(s, x) = \frac{1}{(2\pi\sigma^2)^{|B_s|/2}} \frac{1}{\sqrt{\det(I + \Sigma_o S_3 / \sigma^2)}} \exp \left\{ -\frac{E_s}{2\sigma^2} \right\}, \quad (24)$$

where  $I$  is the identity matrix and  $E_s$  is given by:

$$E_s = \mathbf{s}_1 + \sigma^2 \mu_o^\top \Sigma_o^{-1} \mu_o - (\mathbf{s}_2 + \sigma^2 \Sigma_o^{-1} \mu_o)^\top (S_3 + \sigma^2 \Sigma_o^{-1})^{-1} (\mathbf{s}_2 + \sigma^2 \Sigma_o^{-1} \mu_o). \quad (25)$$

*Proof.* For the AR model of (22),

$$p(x_i | T, \theta_s, x_{-D+1}^{i-1}) = \frac{1}{\sqrt{2\pi\sigma^2}} \exp \left\{ -\frac{1}{2\sigma^2} (x_i - \theta_s^\top \tilde{\mathbf{x}}_{i-1})^2 \right\},$$

so that,

$$\prod_{i \in B_s} p(x_i | T, \theta_s, x_{-D+1}^{i-1}) = \frac{1}{(\sqrt{2\pi\sigma^2})^{|B_s|}} \exp \left\{ -\frac{1}{2\sigma^2} \sum_{i \in B_s} (x_i - \theta_s^\top \tilde{\mathbf{x}}_{i-1})^2 \right\}.$$

Expanding the sum in the exponent gives,

$$\begin{aligned} \sum_{i \in B_s} (x_i - \theta_s^\top \tilde{\mathbf{x}}_{i-1})^2 &= \sum_{i \in B_s} x_i^2 - 2\theta_s^\top \sum_{i \in B_s} x_i \tilde{\mathbf{x}}_{i-1} + \theta_s^\top \sum_{i \in B_s} \tilde{\mathbf{x}}_{i-1} \tilde{\mathbf{x}}_{i-1}^\top \theta_s \\ &= s_1 - 2\theta_s^\top \mathbf{s}_2 + \theta_s^\top S_3 \theta_s, \end{aligned}$$

from which we obtain that,

$$\prod_{i \in B_s} p(x_i | T, \theta_s, x_{-D+1}^{i-1}) = \frac{1}{(\sqrt{2\pi}\sigma^2)^{|B_s|}} \exp \left\{ -\frac{1}{2\sigma^2} (s_1 - 2\theta_s^\top \mathbf{s}_2 + \theta_s^\top S_3 \theta_s) \right\} = (\sqrt{2\pi})^p \rho_s \mathcal{N}(\theta_s; \boldsymbol{\mu}, S),$$

by completing the square, where  $\boldsymbol{\mu} = S_3^{-1} \mathbf{s}_2$ ,  $S = \sigma^2 S_3^{-1}$ , and,

$$\rho_s = \sqrt{\frac{\det(\sigma^2 S_3^{-1})}{(2\pi\sigma^2)^{|B_s|}}} \exp \left\{ -\frac{1}{2\sigma^2} (s_1 - \mathbf{s}_2^\top S_3^{-1} \mathbf{s}_2) \right\}. \quad (26)$$

So, multiplying with the prior:

$$\prod_{i \in B_s} p(x_i | T, \theta_s, x_{-D+1}^{i-1}) \pi(\theta_s) = (\sqrt{2\pi})^p \rho_s \mathcal{N}(\theta_s; \boldsymbol{\mu}, S) \mathcal{N}(\theta_s; \mu_o, \Sigma_o) = \rho_s Z_s \mathcal{N}(\theta_s; \mathbf{m}, \Sigma),$$

where  $\Sigma^{-1} = \Sigma_o^{-1} + S^{-1}$ ,  $\mathbf{m} = \Sigma (\Sigma_o^{-1} \mu_o + S^{-1} \boldsymbol{\mu})$ , and,

$$Z_s = \frac{1}{\sqrt{\det(\Sigma_o + \sigma^2 S_3^{-1})}} \exp \left\{ -\frac{1}{2} (\mu_o - S_3^{-1} \mathbf{s}_2)^\top (\Sigma_o + \sigma^2 S_3^{-1})^{-1} (\mu_o - S_3^{-1} \mathbf{s}_2) \right\}. \quad (27)$$

Therefore,

$$\prod_{i \in B_s} p(x_i | T, \theta_s, x_{-D+1}^{i-1}) \pi(\theta_s) = \rho_s Z_s \mathcal{N}(\theta_s; \mathbf{m}, \Sigma), \quad (28)$$

and hence,

$$P_e(s, x) = \int \prod_{i \in B_s} p(x_i | T, \theta_s, x_{-D+1}^{i-1}) \pi(\theta_s) d\theta_s = \rho_s Z_s.$$

Using standard matrix inversion properties, after some algebra the product  $\rho_s Z_s$  can be rearranged to give exactly the required expression in (24), completing the proof.  $\square$

## B.2 Proof of Lemma 1

Now, we move back to the original case, as described in the paper, where the noise variance is considered to be a parameter of the AR model, so that  $\theta_s = (\boldsymbol{\phi}_s, \sigma_s^2)$ . Here, the joint prior on the parameters is  $\pi(\theta_s) = \pi(\boldsymbol{\phi}_s | \sigma_s^2) \pi(\sigma_s^2)$ , where,

$$\sigma_s^2 \sim \text{Inv-Gamma}(\tau, \lambda), \quad (29)$$

$$\boldsymbol{\phi}_s | \sigma_s^2 \sim \mathcal{N}(\mu_o, \sigma_s^2 \Sigma_o), \quad (30)$$

and where  $(\tau, \lambda, \mu_o, \Sigma_o)$  are hyperparameters.

For  $P_e(s, x)$ , we just need to compute the integral:

$$P_e(s, x) = \int \prod_{i \in B_s} p(x_i | T, \theta_s, x_{-D+1}^{i-1}) \pi(\theta_s) d\theta_s \quad (31)$$

$$= \int \pi(\sigma_s^2) \left( \int \prod_{i \in B_s} p(x_i | T, \phi_s, \sigma_s^2, x_{-D+1}^{i-1}) \pi(\phi_s | \sigma_s^2) d\phi_s \right) d\sigma_s^2. \quad (32)$$

The inner integral has exactly the form of the estimated probabilities  $P_e(s, x)$  from the previous section, where the noise variance was fixed. The only difference is that the prior  $\pi(\phi_s | \sigma_s^2)$  of (30) now has covariance matrix  $\sigma_s^2 \Sigma_o$  instead of  $\Sigma_o$ . So, using (24)-(25), with  $\Sigma_o$  replaced by  $\sigma_s^2 \Sigma_o$ , we get,

$$P_e(s, x) = \int \pi(\sigma_s^2) \left\{ C_s^{-1} \left( \frac{1}{\sigma_s^2} \right)^{|B_s|/2} \exp \left( - \frac{D_s}{2\sigma_s^2} \right) \right\} d\sigma_s^2,$$

with  $C_s$  and  $D_s$  as in Lemma 1. And using the inverse-gamma prior  $\pi(\sigma_s^2)$  of (29),

$$P_e(s, x) = C_s^{-1} \frac{\lambda^\tau}{\Gamma(\tau)} \int \left( \frac{1}{\sigma_s^2} \right)^{\tau'+1} \exp \left( - \frac{\lambda'}{\sigma_s^2} \right) d\sigma_s^2, \quad (33)$$

with  $\tau' = \tau + \frac{|B_s|}{2}$  and  $\lambda' = \lambda + \frac{D_s}{2}$ .

The integral in (33) has the form of an inverse-gamma density with parameters  $\tau'$  and  $\lambda'$ . Its closed-form solution, as required, completes the proof of the lemma:

$$P_e(s, x) = C_s^{-1} \frac{\lambda^\tau}{\Gamma(\tau)} \frac{\Gamma(\tau')}{(\lambda')^{\tau'}}.$$

□

### B.3 Proof of Lemma 2

In order to derive the required expressions for the posterior distributions of  $\phi_s$  and  $\sigma_s^2$ , for a leaf  $s$  of model  $T$ , first consider the joint posterior  $\pi(\theta_s | T, x) = \pi(\phi_s, \sigma_s^2 | T, x)$ , given by,

$$\pi(\theta_s | T, x) \propto p(x | T, \theta_s) \pi(\theta_s) = \prod_{i=1}^n p(x_i | T, \theta_s, x_{-D+1}^{i-1}) \pi(\theta_s) \propto \prod_{i \in B_s} p(x_i | T, \theta_s, x_{-D+1}^{i-1}) \pi(\theta_s),$$

where we used the fact that, in the product, only the terms involving indices  $i \in B_s$  are functions of  $\theta_s$ . So,

$$\pi(\phi_s, \sigma_s^2 | T, x) \propto \left( \prod_{i \in B_s} p(x_i | T, \phi_s, \sigma_s^2, x_{-D+1}^{i-1}) \pi(\phi_s | \sigma_s^2) \right) \pi(\sigma_s^2).$$

Here, the first two terms can be computed from (28) of the previous section, where the noise variance was known. Again, the only difference is that we have to replace  $\Sigma_o$  with  $\sigma_s^2 \Sigma_o$  because of the prior  $\pi(\phi_s | \sigma_s^2)$  defined in (30). After some algebra, this gives,

$$\pi(\phi_s, \sigma_s^2 | T, x) \propto \left( \frac{1}{\sigma_s^2} \right)^{|B_s|/2} \exp \left( - \frac{D_s}{2\sigma_s^2} \right) \mathcal{N}(\phi_s; \mathbf{m}_s, \Sigma_s) \pi(\sigma_s^2),$$

with  $\mathbf{m}_s$  defined as in Lemma 2, and  $\Sigma_s = \sigma_s^2 (S_3 + \Sigma_o^{-1})^{-1}$ .

Substituting the prior  $\pi(\sigma_s^2)$  in the last expression,

$$\pi(\phi_s, \sigma_s^2 | T, x) \propto \left( \frac{1}{\sigma_s^2} \right)^{\tau+1+|B_s|/2} \exp \left( - \frac{\lambda + D_s/2}{\sigma_s^2} \right) \mathcal{N}(\phi_s; \mathbf{m}_s, \Sigma_s). \quad (34)$$

From (34), it is easy to integrate out  $\phi_s$  and get the posterior of  $\sigma_s^2$ ,

$$\pi(\sigma_s^2 | T, x) = \int \pi(\phi_s, \sigma_s^2 | T, x) d\phi_s \propto \left( \frac{1}{\sigma_s^2} \right)^{\tau+1+|B_s|/2} \exp \left( - \frac{\lambda + D_s/2}{\sigma_s^2} \right),$$

which is of the form of an inverse-gamma distribution with parameters  $\tau' = \tau + \frac{|B_s|}{2}$  and  $\lambda' = \lambda + \frac{D_s}{2}$ , proving the first part of the lemma.

However, as  $\Sigma_s$  is a function of  $\sigma_s^2$ , integrating out  $\sigma_s^2$  requires more algebra. We have,

$$\begin{aligned} \mathcal{N}(\phi_s; \mathbf{m}_s, \Sigma_s) &\propto \frac{1}{\sqrt{\det(\Sigma_s)}} \exp \left\{ - \frac{1}{2} (\phi_s - \mathbf{m}_s)^T \Sigma_s^{-1} (\phi_s - \mathbf{m}_s) \right\} \\ &\propto \left( \frac{1}{\sigma_s^2} \right)^{p/2} \exp \left\{ - \frac{1}{2\sigma_s^2} (\phi_s - \mathbf{m}_s)^T (S_3 + \Sigma_o^{-1}) (\phi_s - \mathbf{m}_s) \right\}, \end{aligned}$$

and substituting this in (34) gives,

$$\pi(\phi_s, \sigma_s^2 | T, x) \propto \left( \frac{1}{\sigma_s^2} \right)^{\tau+1+\frac{|B_s|+p}{2}} \exp \left\{ - \frac{1}{2\sigma_s^2} \left( 2\lambda + D_s + (\phi_s - \mathbf{m}_s)^T (S_3 + \Sigma_o^{-1}) (\phi_s - \mathbf{m}_s) \right) \right\},$$

which as a function of  $\sigma_s^2$  has the form of an inverse-gamma density, allowing us to integrate out  $\sigma_s^2$ . Denoting  $L = 2\lambda + D_s + (\phi_s - \mathbf{m}_s)^T (S_3 + \Sigma_o^{-1}) (\phi_s - \mathbf{m}_s)$ , and  $\tilde{\tau} = \tau + \frac{|B_s|+p}{2}$ ,

$$\pi(\phi_s | T, x) = \int \pi(\phi_s, \sigma_s^2 | T, x) d\sigma_s^2 \propto \int \left( \frac{1}{\sigma_s^2} \right)^{\tilde{\tau}+1} \exp \left( - \frac{L}{2\sigma_s^2} \right) d\sigma_s^2 = \frac{\Gamma(\tilde{\tau})}{(L/2)^{\tilde{\tau}}}.$$

So, as a function of  $\phi_s$ , the posterior  $\pi(\phi_s | T, x)$  is,

$$\begin{aligned} \pi(\phi_s | T, x) &\propto L^{-\tilde{\tau}} = \left( 2\lambda + D_s + (\phi_s - \mathbf{m}_s)^T (S_3 + \Sigma_o^{-1}) (\phi_s - \mathbf{m}_s) \right)^{-\frac{2\tau+|B_s|+p}{2}} \\ &\propto \left( 1 + \frac{1}{2\tau + |B_s|} (\phi_s - \mathbf{m}_s)^T \frac{(S_3 + \Sigma_o^{-1})(2\tau + |B_s|)}{(2\lambda + D_s)} (\phi_s - \mathbf{m}_s) \right)^{-\frac{2\tau+|B_s|+p}{2}} \\ &\propto \left( 1 + \frac{1}{\nu} (\phi_s - \mathbf{m}_s)^T P_s^{-1} (\phi_s - \mathbf{m}_s) \right)^{-\frac{\nu+p}{2}}, \end{aligned}$$

which is exactly in the form of a multivariate  $t$ -distribution, with  $p$  being the dimension of  $\phi_s$ , and with  $\nu$ ,  $\mathbf{m}_s$  and  $P_s$  exactly as given in Lemma 2, completing the proof.  $\square$

## C Simulated data

The model fitted from  $n = 10^4$  observations is shown here with its MAP estimated parameters:

$$x_n = \begin{cases} 0.68 x_{n-1} - 0.29 x_{n-2} + e_n, & e_n \sim \mathcal{N}(0, 0.15), & \text{if } x_{n-1} > 0, \\ -0.34 x_{n-1} - 0.19 x_{n-2} + e_n, & e_n \sim \mathcal{N}(0, 0.10), & \text{if } x_{n-1} \leq 0, x_{n-2} > 0, \\ 0.49 x_{n-1} + 0.00 x_{n-2} + e_n, & e_n \sim \mathcal{N}(0, 0.050), & \text{if } x_{n-1} \leq 0, x_{n-2} \leq 0. \end{cases}$$

We also report the standard deviation (SD) of the posterior. For each AR coefficient, this can be easily calculated from the multivariate- $t$  posterior of Lemma 2,  $\pi(\phi_s|T, x)$ . The resulting SD “error bars” from the datasets with size  $n = 1000$  and  $n = 10^4$  are reported in Table 4. As expected, with more samples the mode of the posterior moves closer to the true value, and its standard deviation is reduced.

Table 4: Error bars for the estimated AR coefficients

	$s = 1$		$s = 01$		$s = 00$	
True value	<b>0.70</b>	<b>-0.30</b>	<b>-0.30</b>	<b>-0.20</b>	<b>0.50</b>	<b>0.00</b>
MAP estimate	0.66	-0.19	-0.39	-0.27	0.45	-0.03
Posterior SD	0.043	0.043	0.084	0.085	0.065	0.061

(a)  $n = 1000$  observations

True value	<b>0.70</b>	<b>-0.30</b>	<b>-0.30</b>	<b>-0.20</b>	<b>0.50</b>	<b>0.00</b>
MAP estimate	0.68	-0.29	-0.34	-0.19	0.49	0.00
Posterior SD	0.014	0.014	0.024	0.026	0.020	0.019

(b)  $n = 10^4$  observations

## D The IBM stock price

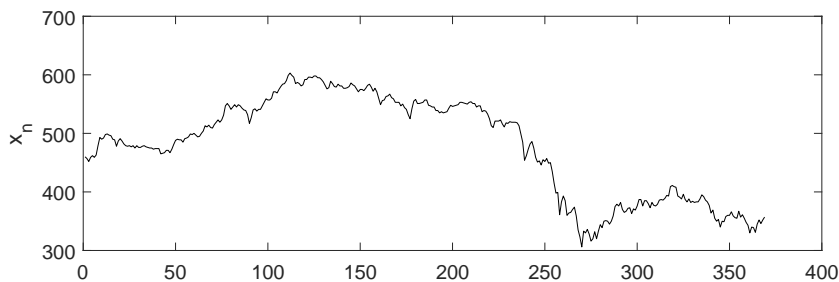


Figure 3: The IBM stock price time series

### D.1 Other models considered

As the most successful among earlier approaches is the MAR model of Wong & Li (2000), we follow the procedure of Wong & Li (2000) for comparing with ARIMA, SETAR and MAR models. The GMTD model considered in Wong & Li (2000) belongs in the class of MAR models as a special case, with the fitted MAR model determined to be superior overall because of its

BIC score. The results shown in Section 4.2 (Table 2) for the ARIMA, SETAR and MAR models are taken from [Wong & Li \(2000\)](#). The corresponding models are:

$$\begin{aligned} \text{ARIMA: } x_n &= x_{n-1} + e_n - 0.09 e_{n-1}, \quad e_n \sim \mathcal{N}(0, 52.2), \\ \text{SETAR: } x_n &= \begin{cases} 1.0452 x_{n-1} - 0.0452 x_{n-2} + e_n, & e_n \sim \mathcal{N}(0, 58.43), & \text{if } x_{n-1} \leq x_{n-2}, \\ 1.1467 x_{n-1} - 0.1467 x_{n-2} + e_n, & e_n \sim \mathcal{N}(0, 45.05), & \text{if } x_{n-1} > x_{n-2}, \end{cases} \\ \text{MAR: } F(x_n|x^{n-1}) &= 0.54 \Phi\left(\frac{x_n - 0.68x_{n-1} - 0.32x_{n-2}}{4.82}\right) \\ &\quad + 0.42 \Phi\left(\frac{x_n - 1.67x_{n-1} + 0.67x_{n-2}}{6.00}\right) + 0.04 \Phi\left(\frac{x_n - x_{n-1}}{18.2}\right). \end{aligned}$$

## D.2 Fitting the BCT-AR model

The details of the procedure (outlined in Section 3.2) followed to select the hyperparameters, AR order and quantiser thresholds, are described here. First, for the hyperparameter  $\beta$  we use the default value  $\beta = 3/4$  for ternary alphabets ([Kontoyiannis et al., 2020](#)), and as usual take  $D = 10, \mu_o = 0, \Sigma_o = I$ . For the inverse-gamma prior, following Section 3.2, we take  $\lambda = 50, \tau = 0.1$ , so that the mode of the inverse-gamma prior,  $\lambda/(\tau + 1)$ , is roughly in a sensible range (for example, the fitted SETAR and ARIMA models have variance close to 40-60).

For the thresholds  $c_1$  and  $c_2$  of the ternary quantiser, we perform a grid search between the 10% and 90% quantiles of the data. In order to reduce the number of runs required in the grid search, we look only at symmetric quantisers, which would naturally be expected for stock prices. We choose  $c = c_2 = -c_1$ , so that  $s = 1$  if  $-c \leq \Delta x_{n-1} \leq c$ , and perform a grid search for  $c$ . At this point, for the AR order of the first-difference series  $\Delta x_n$ , we are using  $p = 1$ , which was identified from the previous models. As shown in Table 5, the evidence  $p(x|c, p)$  is maximised at  $c = 7.0$ .

Table 5: Using the evidence  $p(x|c, p)$  to choose the quantiser threshold

	Threshold $c$							
	1.0	2.0	3.0	4.0	5.0	6.0	7.0	8.0
$-\log_2 p(x c, p)$	1768.5	1768.5	1767.6	1756.9	1757.5	1740.3	<b>1740.0</b>	1760.9

Finally, using the chosen value  $c = 7.0$ , we select the AR order using our Bayesian procedure, considering values in the range  $1 \leq p \leq 5$ . From Table 6, it is indeed verified that the evidence  $p(x|c, p)$  is maximised at  $p = 1$ , identifying the same AR order with other methods. This completes the specification of the training details for the first-difference series  $\Delta x_n$ . The resulting model for the original time series  $x_n$  (which has order  $p = 2$ ), is shown in Section 4.2.

Table 6: Using the evidence  $p(x|c, p)$  to choose the AR order

	AR order $p$				
	1	2	3	4	5
$-\log_2 p(x c, p)$	<b>1740.0</b>	1766.6	1781.6	1788.7	1795.7

## E The US unemployment rate

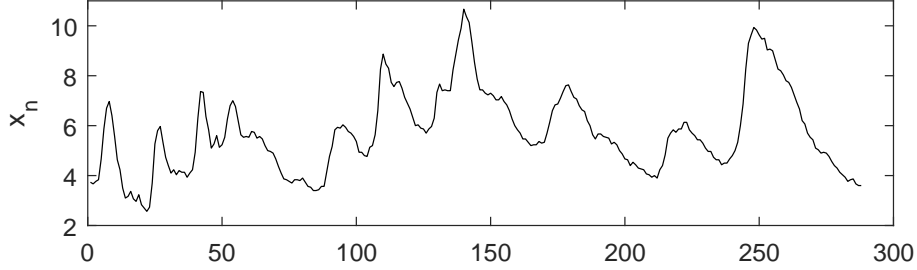


Figure 4: The quarterly US unemployment rate, in the period 1948-2019

### E.1 The SETAR model

The SETAR model fitted to the time series is very similar to that of [Montgomery et al. \(1998\)](#), which was selected from the same data restricted to the shorter time period 1948-1993, with only slightly adjusted parameters. The exact model of [Montgomery et al. \(1998\)](#) is:

$$\Delta x_n = \begin{cases} 0.01 + 0.73 \Delta x_{n-1} + 0.10 \Delta x_{n-2} + e_n, & e_n \sim \mathcal{N}(0, 0.076), & \text{if } \Delta x_{n-2} \leq 0.1, \\ 0.18 + 0.80 \Delta x_{n-1} - 0.56 \Delta x_{n-2} + e_n, & e_n \sim \mathcal{N}(0, 0.165), & \text{if } \Delta x_{n-2} > 0.1. \end{cases}$$

The SETAR model fitted here from the longer time period 1948-2019 is:

$$\Delta x_n = \begin{cases} -0.01 + 0.58 \Delta x_{n-1} + 0.07 \Delta x_{n-2} + e_n, & e_n \sim \mathcal{N}(0, 0.045), & \text{if } \Delta x_{n-2} \leq 0.07, \\ 0.24 + 0.90 \Delta x_{n-1} - 0.67 \Delta x_{n-2} + e_n, & e_n \sim \mathcal{N}(0, 0.136), & \text{if } \Delta x_{n-2} > 0.07. \end{cases}$$

The model was fitted using the R package TSA ([Chan & Ripley, 2020](#)) along with the commonly used conditional least squares method of [Chan \(1993\)](#). The standard errors of the coefficients of regime 1 were 0.021, 0.067 and 0.086, respectively, and those of regime 2 were 0.062, 0.098, and 0.127, respectively.

### E.2 Fitting the BCT-AR model

In this example, following [Montgomery et al. \(1998\)](#), we include a constant term in the AR model, so that,

$$x_n = \phi_{s,0} + \phi_{s,1}x_{n-1} + \dots + \phi_{s,p}x_{n-p} + e_n = \boldsymbol{\phi}_s^T \tilde{\mathbf{x}}_{n-1} + e_n, \quad e_n \sim \mathcal{N}(0, \sigma_s^2).$$

Using  $\boldsymbol{\phi}_s = (\phi_{s,0}, \dots, \phi_{s,p})^T$ , and  $\tilde{\mathbf{x}}_{n-1} = (1, x_{n-1}, \dots, x_{n-p})^T$ , the remaining analysis remains identical.

Table 7: Using the evidence  $p(x|c, p)$  to choose the quantiser threshold

	Threshold $c$									
	-0.2	-0.15	-0.1	-0.05	0.0	0.05	0.1	0.15	0.2	0.25
$-\log_2 p(x c, p)$	77.1	60.3	60.3	45.7	55.5	49.2	48.8	<b>39.9</b>	46.4	43.0

The hyperparameter values used here are  $\beta = 0.5$ ,  $D = 10$ ,  $\mu_o = 0$ ,  $\Sigma_o = I$ ,  $\lambda = 0.1$ ,  $\tau = 0.1$ . In order to select the threshold of the binary quantiser, we perform a grid search similarly with the previous example. As shown in Table 7, the evidence  $p(x|c, p)$  is maximised at  $c = 0.15$ . For the prediction experiment, the same procedure was applied to the training set (consisting of the first 50% of the observations). The selected quantiser threshold was again  $c = 0.15$ .

### E.3 Error bars

The posterior standard deviations (SD) around the MAP estimates are reported in Table 8 for the AR coefficients of the BCT-AR model of Section 4.3.

Table 8: Error bars for the estimated AR coefficients

	$s = 1$			$s = 01$			$s = 00$		
MAP estimate	0.09	0.72	-0.30	0.04	0.29	-0.32	-0.02	0.34	0.19
Posterior SD	0.09	0.16	0.13	0.10	0.24	0.23	0.02	0.07	0.07